

Multimer analysis method reveals higher-order topology in quasicrystals

Aoqian Shi, Jiapei Jiang, Yuchen Peng, Peng Peng, Jianzhi Chen, and Jianjun Liu*

Key Laboratory for Micro/Nano Optoelectronic Devices of Ministry of Education & Hunan Provincial Key Laboratory of Low-Dimensional Structural Physics and Devices, School of Physics and Electronics, Hunan University, Changsha 410082, China

*Corresponding author: jianjun.liu@hnu.edu.cn

ABSTRACT: Higher-order topological insulator (HOTI) has been extended from crystals to quasicrystals. However, due to the difference in spatial symmetry, the realization mechanism and analysis method of HOTI in crystals and quasicrystals are not universal. In this Letter, the multimer analysis method (MAM) is strictly defined and improved, and the higher-order topology (HOT) in quasicrystals is revealed by MAM and its universality in crystals is verified. The Stampfli-type higher-order topological quasicrystalline insulator (HOTQI) protected by long-range C_{12} symmetry dominated by C_6 symmetry is constructed. Based on MAM, the topological phase transition of HOTQI is investigated, and a real-space topological index is proposed. In addition, photonic and phononic analogs of HOTQI are constructed based on MAM. This work provides a universal method for revealing the HOT in various systems (crystals and quasicrystals, electronics, photonics and phononics).

Keywords: multimer analysis method; higher-order topological insulator; higher-order topological quasicrystalline insulator

1. Introduction

Different from topological insulators based on time-reversal symmetry, particle-hole symmetry, and chiral symmetry [1,2], topological crystalline insulator (TCI) based on the spatial symmetries (such as rotation symmetry and mirror symmetry) plays a unique role in fundamental and applied physics[3–5]. In recent years, as an important branch of TCI, higher-order topological insulator (HOTI) has attracted extensive

attention [6–29]. The difference (d) of physical dimension between bulk system and topological states in HOTI satisfies $d > 1$. HOTI has been theoretically and experimentally verified in electronics [6–14], photonics [15–23] and phononics [24–29]. In addition, HOTI provides an excellent platform for studying novel physical phenomena such as bound states in the continuum [30], dislocation states [31,32], disclination states [33–36] and screw dislocation states [37].

In recent years, the research of topological effects has been extended to one-dimensional quasicrystals (quasi-periodic systems) with irrational number sequences [38–41] and two-dimensional quasicrystals (quasi-periodic systems) with rotation symmetry, self-similarity and long-range order [42–45]. Higher-order topological quasicrystalline insulator (HOTQI) based on quasicrystals exhibits unique charms that periodic systems do not possess (such as higher-order topological states protected by C_5 , C_8 , and C_{12} symmetry) [46–51]. However, affected by the different rotation symmetry and whether there is translation symmetry, HOTQI (HOTI) generally adopts the model of multi-orbital atoms (single-orbital atoms) and needs (does not need) to introduce additional mass terms. The difference in the realization mechanisms makes the analysis methods of HOTQI and HOTI not universal. The analysis methods of HOTQI based on effective edge theory [47,48] or fractional mass kinks [49,51] are too complicated for crystals. The analysis methods of HOTI based on Wannier functions and Wannier centers [12,13] are limited by the translation symmetry and cannot be extended to quasicrystals. Although the quasicrystalline quadrupole topological insulator without additional mass term has been theoretically and experimentally verified [52], it needs to introduce negative couplings, which makes it inconvenient to extend to photonics and phononics, limiting its application. Therefore, it is urgent to establish an analysis method suitable for various systems (crystals and quasicrystals, electronics, photonics and phononics) to characterize the higher-order topology (HOT). Previous HOTI [11,15,19] and recent research on the HOT in fractal lattice [29] have considered the limiting case where intracell hopping is vanishing, and the system can be regarded as the combination of multimers. Multimer provides a convenient and effective way to analyze the topology in the

system, and the multimer is not limited by the translation symmetry of the system, which is expected to be used to analyze the HOT in quasicrystals. However, previous researches have only focused on individual multimers and systems, the definitions of multimers and corresponding analysis method are incomplete, and the applicability of analysis method in various systems is unclear.

In this Letter, the multimer analysis method (MAM) is strictly defined and improved and its universality in systems with different symmetries is verified. The Stampfli-type HOTQI protected by symmetry C_{Stampfli} (long-range C_{12} symmetry dominated by C_6 symmetry) is constructed. Combined with the tight-binding Hamiltonian and MAM, the HOT and topological phase transition of HOTQI are investigated, and a real-space topological index is proposed. The photonic and phononic analogs of HOTQI (i.e., photonic and phononic HOTQI) are proposed and realized, which provide theoretical basis for the experimental verification of photonic and phononic HOTQI.

2. Model and theory

In this Letter, the ensemble of n ($n > 1$) single-orbital atoms that are equidistantly connected (interacting) to form a closed shape is called a multimer, which satisfies C_n symmetry. When $n = 1$, the isolated atom is called a monomer, which is a special multimer. The multimers and their electronic types are shown in Fig. 1.

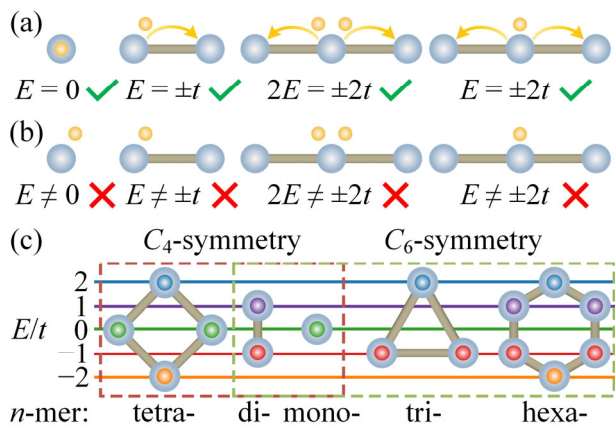


Fig. 1. Multimers and their electronic types. (a) Types of electrons that can exist in multimers. Light blue (yellow) spheres correspond to atoms (electrons) in multimers, and yellow arrows indicate the transition of electrons between neighboring atoms. (b) Types of electrons that cannot

exist in multimers. (c) Multimers satisfying C_4 and C_6 symmetry. Colored spheres correspond to electrons with different energies.

The hopping strength of electrons between adjacent atoms in the multimer is denoted as t ($t \geq 0$). Without loss of generality, let $t = 1$ ($t = 0$) when the hopping exists (vanishes). Regardless of the spin degree of freedom, the effective Hamiltonian describing the dynamics of the electron in the multimer is,

$$\begin{aligned} H_1 &= 0, H_2 = t\sigma_x \\ H_n &= \sum_{s=1}^n (t|(s \bmod n) + 1\rangle\langle s| + h.c.), \quad n \geq 3 \end{aligned} \quad (1)$$

where $|s\rangle$ is the electronic state of the atom s ($1 \leq s \leq n$), and σ_x is the Pauli matrix.

According to $H|\psi\rangle = E|\psi\rangle$, the eigenvalues corresponding to the multimer can be obtained. In addition, the electron type (charge c and energy E) of the multimer can also be obtained by using the energy matching and energy conservation. When the multimer is half-filled (filling $n/2$ electrons with $E \leq 0$), assuming that the electron with charge c_s and energy E_s exists in the orbital of atom s , the total energy of the electron should match the energy corresponding to the hopping, as shown in Figs. 1(a) and 1(b). When the multimer is fully filled (filling n electrons), the total energy of multimer is zero because the energy of atoms themselves is not considered and the multimer is an adiabatic system. The number of atoms interacting with atom s (i.e., electron hopping between adjacent atoms) is denoted as l_s , $l_s = 0, 1$ and 2 correspond to $n = 1, 2$ and $n \geq 3$, respectively. According to the energy relationship, the electronic type satisfies,

$$c_s |E_s| = l_s t, \quad \sum_{s=1}^n E_s = 0 \quad (2)$$

In this Letter, the multimers ($n = 1, 2, 3, 4, 6$) satisfying C_4 and C_6 symmetry are mainly considered, and their corresponding electronic types can be obtained by Eq. (2), as shown in Fig. 1(c). The energy spectrum and charge density of a system composed of multimers can be qualitatively and quantitatively obtained by the multimers and their corresponding electron types, and the topology in the system can

be effectively analyzed [11,15,19,29]. In this Letter, the method is called MAM, and its applicability in HOTI satisfying C_4 and C_6 symmetry is verified (see Part I of Supplementary Material [53]), and it is applied to complicated quasi-periodic systems, demonstrating the universality of MAM.

3. Results and discussion

Using an iterative subdivision method, with squares and equilateral triangles as primitive tiles, a Stampfli-type quasicrystal tiling can be constructed (see Part II of Supplementary Material [53]). The vertex of each primitive tile (i.e., the lattice site of quasicrystal) is used as a basic cell, which contains six subsites. Subsites can place scatterers corresponding to electronics, photonics and phononics. The tiling can be transformed into the corresponding tight-binding model. Stampfli-type normal insulator (NI) and HOTQI are shown in Fig. 2.

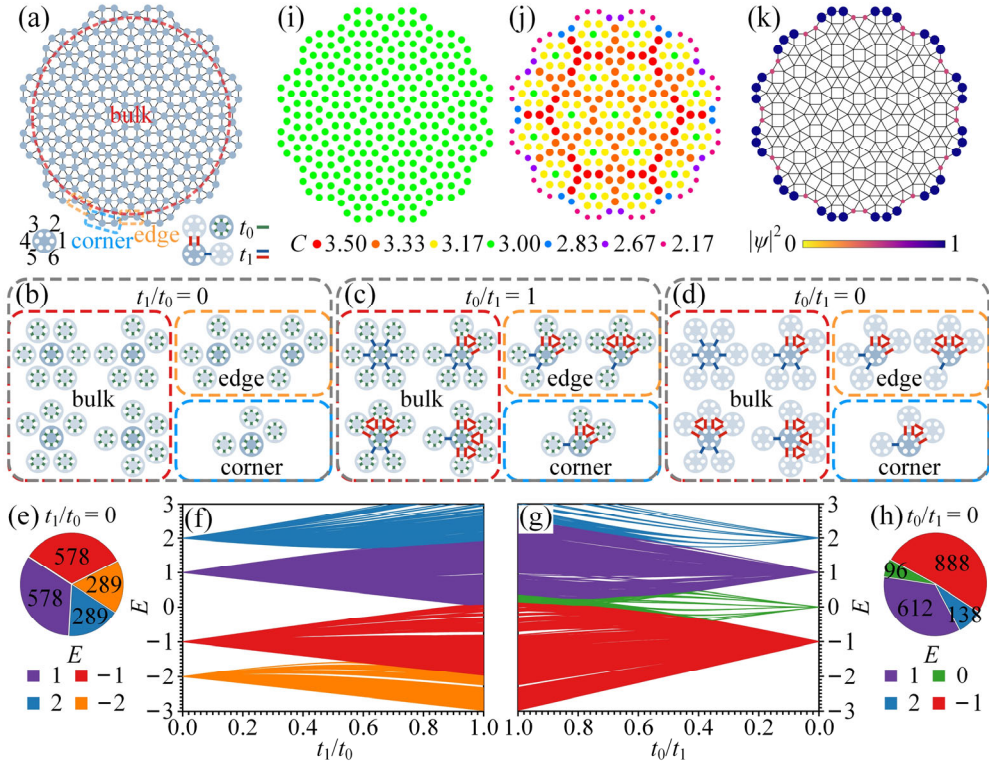


Fig. 2. Stampfli-type NI and HOTQI. (a) The tight-binding model of the Stampfli-type quasicrystal consists of 289 basic cells. The dashed boxes correspond to the bulk, edge, and corner regions. The lower left illustration is the serial number of subsites in the basic cell, and the lower right illustration is a schematic of the hopping term within the basic cell (hopping strength t_0) and between the adjacent basic cells (hopping strength t_1). (b)–(d) Multimer types in Stampfli-type

quasicrystal and their variations with t_1/t_0 and t_0/t_1 . (e)–(h) Energy spectrum of eigenvalues: (e) and (f) $0 \leq t_1/t_0 \leq 1$, (g) and (h) $0 \leq t_0/t_1 \leq 1$. (i) and (j) Charge density: (i) $t_1 = 0, t_0 = 1$, (j) $t_0 = 0, t_1 = 1$. (k) Normalized probability distribution of the wave function for $t_0 = 0, t_1 = 1$ and $E = 0$.

As a finite-size system, the tight-binding Hamiltonian of the Stampfli-type quasicrystal in Fig. 2(a) can be expressed as,

$$H_{\text{Stampfli}} = \sum_i c_i^\dagger t_0 h_0 c_i + \sum_{\langle i,j \rangle} c_i^\dagger t_1 h_1 c_j \quad (3)$$

where c_i^\dagger represents the electron creation operator of basic cell i , $c_i(c_j)$ represents the electron annihilation operator of basic cell $i(j)$. h_0 (h_1) is determined by the hopping term within the basic cell (between the basic cells) (see Part III of Supplementary Material [53]). The Stampfli-type quasicrystal satisfies symmetry C_{Stampfli} (see Part III of Supplementary Material [53]).

When $t_0(t_1) = 0$ and $t_1(t_0) \neq 0$, the tight-binding model behaves as a combination of multimers. Since the structure satisfies symmetry C_{Stampfli} , there are hexamers, trimers, dimers, and monomers. The specific forms of the multimers are further analyzed, as shown in Figs. 2(b) and 2(d). The type of multimer in the basic cell of the bulk, edge and corner regions is denoted as Ω , which satisfies,

$$\Omega = (\#H, \#T, \#D, \#M) \quad (4)$$

where $\#H$, $\#T$, $\#D$ and $\#M$ correspond to the number of hexamers, trimers, dimers, and monomers, respectively.

When $t_1 = 0, t_0 = 1$ (i.e., $t_1/t_0 = 0$), the basic cells in the bulk, edge, and corner regions all have $\Omega = (1, 0, 0, 0)$, as shown in Fig. 2(b). The energy spectrum of eigenvalues in Fig. 2(e) is obtained by solving the Hamiltonian. The charge density is shown in Fig. 2(i) by filling the energy band with $E < 0$. All 289 basic cells have charge $C = 3$. According to MAM, 289 (578) electrons with $E = -2$ ($E = -1$) will be filled in 289 hexamers with 3 electrons per hexamer (i.e., $C = 3$), which is consistent with the numerical results. From the same charge density in the bulk, edge, and corner regions, the structure corresponds to the NI with trivial phase.

When $t_0 = 0, t_1 = 1$ (i.e., $t_0/t_1 = 0$), the basic cell has $\Omega = \{(0, 0, 6, 0), (0, 1, 5, 0), (0,$

$(2, 4, 0), (0, 3, 3, 0)\}$, $\Omega = \{(0, 1, 4, 1), (0, 2, 3, 1)\}$, and $\Omega = (0, 1, 3, 2)$ in the bulk, edge and corner region, respectively, as shown in Fig. 2(d). The energy spectrum of eigenvalues in Fig. 2(h) is $E = \{2, \pm 1, 0\}$. Filling the band with $E < 0$, the charge is $C = \{3.5, 3.33, 3.17, 3\}$, $C = \{2.83, 2.67\}$, and $C = 2.17$ in the bulk, edge, and corner region, respectively, as shown in Fig. 2(j). According to MAM, 888 electrons with $E = -1$ will be filled in 138 trimers and 612 dimers, where each trimer is filled with 2 electrons. Since the 3 (2) atoms of the trimer (dimer) are equivalent, the probability of electron filling is the same as 33.3% (50%), so the charge of the basic cell is $C = \#T \times 2 \times 0.333 + \#D \times 0.5$, which is consistent with the numerical results in Fig. 2(j). The fractional value of corner charge is different from that of bulk and edge. According to previous researches on HOTI [12,13] and HOTQI [50,51], this fractional corner anomaly reflects the HOT. From the probability distribution of wave function in Fig. 2(k), it can be found that there are localized states protected by symmetry C_{Stampfli} in the edge and corner regions, which is a sign that the Stampfli-type quasicrystal has HOT, indicating the realization of Stampfli-type HOTQI. It should be noted that the fractional corner anomaly is an external manifestation of the types of multimers in the corner region different from that in the bulk and edge regions.

The topological phase transition and topology of the Stampfli-type HOTQI are further analyzed based on MAM. When t_1/t_0 (t_0/t_1) = 0 changes to $0 < t_1/t_0$ (t_0/t_1) < 1 , that is, the coupling term between (within) the basic cells is not zero, the multimer evolves into the quasi-multimer. As t_1/t_0 (t_0/t_1) (the denominator is 1) gradually increases from zero, the energy spectrum of the eigenvalues gradually broadens. When $t_0 = t_1 = 1$ (i.e., $t_0/t_1 = 1$), the whole structure becomes a complex mixture, the energy gap is closed, and the system is in a critical state. The above processes are shown in Figs. 2(b)–2(d), 2(f) and 2(g), which correspond to the phase transition of the system. Since the system evolves adiabatically in the range of $0 \leq t_1/t_0$ (t_0/t_1) < 1 , and its topology will not change in the corresponding range, the topology of the system can be judged by the limiting case t_1/t_0 (t_0/t_1) = 0 (corresponding to the multimers). For the $1/n$ sector of the C_n symmetric structure, there is no monomer in the bulk region, and the number of monomers in the edge and corner regions are

$\#M_{\text{edge}}$ and $\#M_{\text{corner}}$, respectively, then the total number of monomers in the system is,

$$\#M_{\text{total}} = n \times (\#M_{\text{edge}} + \#M_{\text{corner}}) \quad (5)$$

The electrons with zero energy will be localized in these monomers to form topologically localized states (TLSs), that is, when $E = 0$, the probability distribution of the wave function satisfies $\sum_j |\psi_j|^2 = \#M_{\text{total}}$, and j is the basic cell in the edge and corner regions. Therefore, $\#M$ can be used as a real-space topological index, which is expressed as,

$$\begin{cases} \#M_{\text{total}} = 0, & \text{trivial} \\ \#M_{\text{total}} \neq 0, & \text{nontrivial} \\ \#M_{\text{corner}} \neq 0, & \text{HOTQI (HOTI)} \end{cases} \quad (6)$$

MAM and its real-space topological index provide an effective way to characterize HOT in various systems. HOTQIs with different symmetries are further investigated in this Letter (see Part IV of Supplementary Material [53]).

Photonic crystal is an excellent platform to realize HOTI [15–23]. Similarly, photonic quasicrystal (quasi-periodic photonic crystal) can be used to realize HOTQI, that is, photonic HOTQI. The analysis of its structure and topology is shown in Fig. 3.

As shown in Figs. 3(a) and 3(b), based on the tight-binding model of the Stampfli-type quasicrystal in Fig. 2(a), six circular scatterers are placed at six subsites in each basic cell. The radius of the scatterer is $r = 2.5$ mm, the scatterer material is alumina ceramic ($\epsilon_{r1} = 8.5$), and the background material is air ($\epsilon_{r2} = 1$). The distance between the nearest basic cell is $a = 25$ mm, and the distance d ($d = d_1, d_2, d_3$) between the scatterer and the center of the basic cell corresponds to different multimers, $d_1 = 2r$ (hexamer), $d_2 = a/2 - r$ (dimer), and $d_3 = (a - 2r)/\sqrt{3}$ (trimer) (see Part V of Supplementary Material [53]). It can be seen from Figs. 3(c)–3(j) that in the bandgap of $f \in [6.20\text{GHz}, 7.02\text{GHz}]$ (see Part VI of Supplementary Material [53]), there are 6 kinds of TLSs corresponding to monomers in the edge or corner region, and these TLSs satisfy symmetry C_{Stampfli} . Comparing the results of tight-binding model in Fig. 2(k), due to the finite size effect and the unavoidable long-range coupling in the photonic system, the localized modes in the photonic HOTQI are not completely consistent with the results obtained by the theoretical

model, but its HOT is not affected. Photonic HOTQI has excellent robustness, and its verification results are detailed in Part VII of Supplementary Material [53].

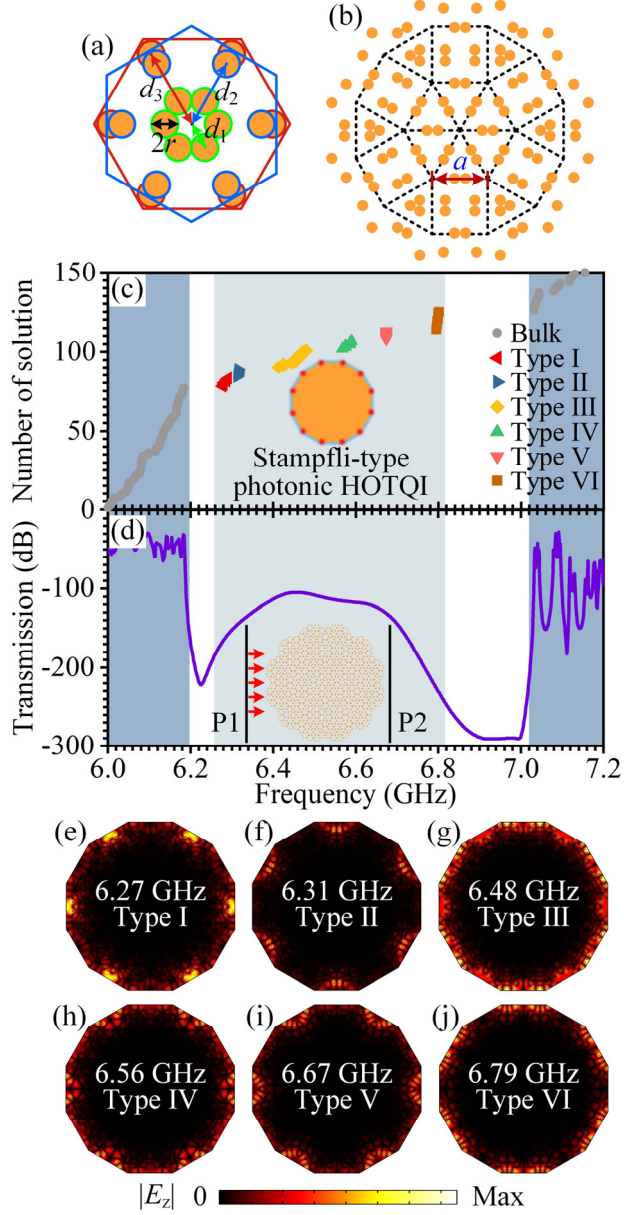


Fig. 3. Stampfli-type photonic HOTQI. (a) Arrangement of scatterers in the basic cell. (b) Schematic diagram of partial basic cells satisfying the Stampfli-type structure. (c) The eigenfrequency distribution illustrated with a schematic of TLSs in the edge and corner regions of the structure. (d) Transmission spectrum illustrated with a schematic of the two-port measurement, P1 (P2) is the input (output) ports. (e)–(j) Eigenmodes corresponding to the TLSs.

In this Letter, phononic HOTQI based on MAM is further investigated and TLSs satisfying symmetry C_{Stampfli} are realized (see Part VIII of Supplementary Material

[53]). MAM provides a convenient, effective, and universal method for analyzing HOT in various systems (crystals and quasicrystals, electronics, photonics and phononics). Photonic and phononic topological insulators have extraordinary application potential, such as high-efficiency lossless optical (acoustic) waveguides [54–56], lasers [57], and audio lasing [58]. The numerical calculation in this work provides a theoretical reference for the experimental verification of photonic and phononic HOTQI and the expansion of their applications in the field of optics and acoustics.

4. Conclusion

In this Letter, MAM is strictly defined and improved. The HOT of Stampfli-type quasicrystal in electronic, photonic and phononic systems has been characterized qualitatively and quantitatively. The applicability of MAM in crystals has also been verified. This work provides a convenient, effective, and universal method for investigating HOT in various systems. The photonic and phononic HOTQI realized in this work broaden the classification of HOTI. They have unique TLSs that satisfy symmetry C_{Stampfli} , which provides a new idea for designing optical and acoustic devices with stronger localization and higher integration degree.

Acknowledgements

The authors thank Xiaokang Dai for helpful discussions. The authors acknowledge Professor J. Q. Liu for software sponsorship. This work is supported by the National Natural Science Foundation of China (Grant Nos. 61405058 and 62075059), the Natural Science Foundation of Hunan Province (Grant Nos. 2017JJ2048 and 2020JJ4161), and the Fundamental Research Funds for the Central Universities (Grant No. 531118040112).

References

- [1] M. Z. Hasan and C. L. Kane, “Colloquium: topological insulators,” *Rev. Mod. Phys.* **82**(4): 3045 (2010).
- [2] X.-L. Qi and S.-C. Zhang, “Topological insulators and superconductors,” *Rev. Mod. Phys.* **83**(4): 1057 (2011).

- [3] L. Fu, “Topological crystalline insulators,” *Phys. Rev. Lett.* **106**(10): 106802 (2011).
- [4] Y. Ando and L. Fu, “Topological crystalline insulators and topological superconductors: From concepts to materials,” *Annu. Rev. Condens. Matter Phys.* **6**: 361–381 (2015).
- [5] C.-K. Chiu, J. C. Y. Teo, A. P. Schnyder, and S. Ryu, “Classification of topological quantum matter with symmetries,” *Rev. Mod. Phys.* **88**(3): 035005 (2016).
- [6] W. A. Benalcazar, B. A. Bernevig, and T. L. Hughes, “Quantized electric multipole insulators,” *Science* **357**(6346): 61–66 (2017).
- [7] W. A. Benalcazar, B. A. Bernevig, and T. L. Hughes, “Electric multipole moments, topological multipole moment pumping, and chiral hinge states in crystalline insulators,” *Phys. Rev. B* **96**(24): 245115 (2017).
- [8] J. Langbehn, Y. Peng, L. Trifunovic, F. von Oppen, and P. W. Brouwer, “Reflection-symmetric second-order topological insulators and superconductors,” *Phys. Rev. Lett.* **119**(24): 246401 (2017).
- [9] Z. Song, Z. Fang, and C. Fang, “(d–2)-dimensional edge states of rotation symmetry protected topological states,” *Phys. Rev. Lett.* **119**(24): 246402 (2017).
- [10] F. Schindler, A. M. Cook, M. G. Vergniory, Z. Wang, S. S. P. Parkin, B. A. Bernevig, and T. Neupert, “Higher-order topological insulators,” *Sci. Adv.* **4**(6): eaat0346 (2018).
- [11] M. Ezawa, “Higher-order topological insulators and semimetals on the breathing kagome and pyrochlore lattices,” *Phys. Rev. Lett.* **120**(2): 026801 (2018).
- [12] W. A. Benalcazar, T. Li, and T. L. Hughes, “Quantization of fractional corner charge in C_n -symmetric higher-order topological crystalline insulators,” *Phys. Rev. B* **99**(24): 245151 (2019).
- [13] C. W. Peterson, T. Li, W. A. Benalcazar, T. L. Hughes, and G. Bahl, “A fractional corner anomaly reveals higher-order topology,” *Science* **368**(6495): 1114–1118 (2020).
- [14] B. Xie, H. Wang, X. Zhang, P. Zhan, J. H. Jiang, M. H. Lu, and Y. F. Chen, “Higher-order band topology,” *Nat. Rev. Phys.* **3**(7): 520–532 (2021).

[15] B. Xie, H. Wang, H. Wang, X. Zhu, J. Jiang, M. Lu, and Y. Chen, “Second-order photonic topological insulator with corner states,” *Phys. Rev. B* **98**(20): 205147 (2018).

[16] J. Noh, W. A. Benalcazar, S. Huang, M. J. Collins, K. P. Chen, T. L. Hughes, and M. C. Rechtsman, “Topological protection of photonic mid-gap defect modes,” *Nat. Photon.* **12**(7): 408–415 (2018).

[17] X. Chen, W. Deng, F. Shi, F. Zhao, M. Chen, and J. Dong, “Direct observation of corner states in second-order topological photonic crystal slabs,” *Phys. Rev. Lett.* **122**(23): 233902 (2019).

[18] B. Xie, G. Su, H. Wang, H. Su, X. Shen, P. Zhan, M. Lu, Z. Wang, and Y. Chen, “Visualization of higher-order topological insulating phases in two-dimensional dielectric photonic crystals,” *Phys. Rev. Lett.* **122**(23): 233903 (2019).

[19] M. Li, D. Zhirihin, M. Gorlach, X. Ni, D. Filonov, A. Slobozhanyuk, A. Alù, and A. B. Khanikaev, “Higher-order topological states in photonic kagome crystals with long-range interactions,” *Nat. Photon.* **14**(2): 89–94 (2020).

[20] A. Shi, B. Yan, R. Ge, J. Xie, Y. Peng, H. Li, W. E. I. Sha, and J. Liu, “Coupled cavity-waveguide based on topological corner state and edge state,” *Opt. Lett.* **46**(5): 1089–1092 (2021).

[21] Y. Wei, B. Yan, Y. Peng, A. Shi, D. Zhao, R. Peng, Y. Xiang, and J. Liu, “Fragile topology in double-site honeycomb lattice photonic crystal,” *Opt. Lett.* **46**(16): 3941–3944 (2021).

[22] J. Jiang, B. Yan, Y. Peng, J. Xie, A. Shi, and J. Liu, “Multiband topological states in non-Hermitian photonic crystals,” *Opt. Lett.* **47**(2): 437–440 (2022).

[23] Y. Peng, E. Liu, B. Yan, J. Xie, A. Shi, P. Peng, H. Li, and J. Liu, “Higher-order topological states in two-dimensional Stampfli-Triangle photonic crystals,” *Opt. Lett.* **47**(12): 3011–3014 (2022).

[24] X. Zhang, H. Wang, Z. Lin, Y. Tian, B. Xie, M. Lu, Y. Chen, and J. Jiang, “Second-order topology and multidimensional topological transitions in sonic crystals,” *Nat. Phys.* **15**(6): 582–588 (2019).

[25] H. Xue, Y. Yang, F. Gao, Y. Chong, and B. Zhang, “Acoustic higher-order topological insulator on a kagome lattice,” *Nat. Mater.* **18**(2): 108–112 (2019).

[26] X. Ni, M. Weiner, A. Alù, and A. B. Khanikaev, “Observation of higher-order topological acoustic states protected by generalized chiral symmetry,” *Nat. Mater.* **18**(2): 113–120 (2019).

[27] Y. Qi, C. Qiu, M. Xiao, H. He, M. Ke, and Z. Liu, “Acoustic realization of quadrupole topological insulators,” *Phys. Rev. Lett.* **124**(20): 206601 (2020).

[28] Z. Yang, X. Lin, Y. Peng, X. Zou, and J. Cheng, “Helical higher-order topological states in an acoustic crystalline insulator,” *Phys. Rev. Lett.* **125**(25): 255502 (2020).

[29] S. Zheng, X. Man, Z. Kong, Z. Lin, G. Duan, N. Chen, D. Yu, J. Jiang, and B. Xia, “Observation of fractal topological states in acoustic metamaterials,” *arXiv:* 2205.04089.

[30] A. Cerjan, M. Jürgensen, W. A. Benalcazar, S. Mukherjee, and M. C. Rechtsman, “Observation of a higher-order topological bound state in the continuum,” *Phys. Rev. Lett.* **125**(21): 213901 (2020).

[31] L. Ye, C. Qiu, M. Xiao, T. Li, J. Du, M. Ke, and Z. Liu, “Topological dislocation modes in three-dimensional acoustic topological insulators,” *Nat. Commun.* **13**(1): 508 (2022).

[32] S. S. Yamada, T. Li, M. Lin, C. W. Peterson, T. L. Hughes, and G. Bahl, “Bound states at partial dislocation defects in multipole higher-order topological insulators,” *Nat. Commun.* **13**(1): 2035 (2022).

[33] T. Li, P. Zhu, W. A. Benalcazar, and T. L. Hughes, “Fractional disclination charge in two-dimensional C_n -symmetric topological crystalline insulators,” *Phys. Rev. B* **101**(11): 115115 (2020).

[34] C. W. Peterson, T. Li, W. Jiang, T. L. Hughes, and G. Bahl, “Trapped fractional charges at bulk defects in topological insulators,” *Nature* **589**(7842): 376–380 (2021).

[35] Y. Liu, S. Liang, F. Li, Z. Lin, X. Tao, Y. Poo, and J. Jiang, “Bulk-disclination correspondence in topological crystalline insulators,” *Nature* **589**(7842): 381–385 (2021).

[36] Y. Deng, W. A. Benalcazar, Z. Chen, M. Oudich, G. Ma, and Y. Jing, “Observation of degenerate zero-energy topological states at disclinations in an

acoustic lattice,” *Phys. Rev. Lett.* **128**(17): 174301 (2022).

[37] Z. Lin, Y. Wu, B. Jiang, Y. Liu, S. Wu, F. Li, and J. Jiang, “Topological Wannier cycles induced by sub-unit-cell artificial gauge flux in a sonic crystal,” *Nat. Mater.* **21**(4): 430–437 (2022).

[38] Y. E. Kraus, Y. Lahini, Z. Ringel, M. Verbin, and O. Zilberberg, “Topological states and adiabatic pumping in quasicrystals,” *Phys. Rev. Lett.* **109**(10): 106402 (2012).

[39] Y. Zhang, L. Xiong, M. Zhang, and X. Jiang, “Fractal topological band-gap structure induced by singularities in the one-dimensional Thue–Morse system,” *Photonics Res.* **9**(4): 622–629 (2021).

[40] O. Zilberberg, “Topology in quasicrystals,” *Opt. Mater. Express* **11**(4): 1143–1157 (2021).

[41] S. Weidemann, M. Kremer, S. Longhi, and A. Szameit, “Topological triple phase transition in non-Hermitian Floquet quasicrystals,” *Nature* **601**(7893): 354–359 (2022).

[42] M. A. Bandres, M. C. Rechtsman, and M. Segev, “Topological photonic quasicrystals: fractal topological spectrum and protected transport,” *Phys. Rev. X* **6**(1): 011016 (2016).

[43] H. Huang and F. Liu, “Quantum spin Hall effect and spin Bott index in a quasicrystal lattice,” *Phys. Rev. Lett.* **121**(12): 126401 (2018).

[44] Z. Che, Y. Zhang, W. Liu, M. Zhao, J. Wang, W. Zhang, F. Guan, X. Liu, W. Liu, L. Shi, and J. Zi, “Polarization singularities of photonic quasicrystals in momentum space,” *Phys. Rev. Lett.* **127**(4): 043901 (2021).

[45] J. Fan and H. Huang, “Topological states in quasicrystals,” *Front. Phys.* **17**(1): 13203 (2022).

[46] D. Varjas, A. Lau, K. Pöyhönen, A. R. Akhmerov, D. I. Pikulin, and I. C. Fulga, “Topological phases without crystalline counterparts,” *Phys. Rev. Lett.* **123**(19): 196401 (2019).

[47] R. Chen, C. Z. Chen, J. H. Gao, B. Zhou, and D. H. Xu, “Higher-order topological insulators in quasicrystals,” *Phys. Rev. Lett.* **124**(3): 036803 (2020).

[48] C. B. Hua, R. Chen, B. Zhou, and D. H. Xu, “Higher-order topological insulator

in a dodecagonal quasicrystal," *Phys. Rev. B* **102**(24): 241102 (2020).

[49] S. Spurrier and N. R. Cooper, "Kane-Mele with a twist: Quasicrystalline higher-order topological insulators with fractional mass kinks," *Phys. Rev. Research* **2**(3): 033071 (2020).

[50] H. Huang, J. Fan, D. Li, and F. Liu, "Generic orbital design of higher-order topological quasicrystalline insulators with odd five-fold rotation symmetry," *Nano Lett.* **21**(16): 7056–7062 (2021).

[51] C. Wang, F. Liu, and H. Huang, "Effective model for fractional topological corner modes in quasicrystals," *Phys. Rev. Lett.* **129**(5): 056403 (2022).

[52] B. Lv, R. Chen, R. Li, C. Guan, B. Zhou, G. Dong, C. Zhao, Y. Li, Y. Wang, H. Tao, J. Shi, and D. H. Xu, "Realization of quasicrystalline quadrupole topological insulators in electrical circuits," *Commun. Phys.* **4**(1): 108 (2021).

[53] See Supplementary Material for details of MAM in NIs and HOTIs satisfying C_4 and C_6 symmetry, construction of Stampfli-type quasicrystal tiling, Hamiltonian and symmetry of Stampfli-type quasicrystal, analysis of HOTQIs with different symmetries, construction of the photonic HOTQI, bandgap of photonic NI and photonic HOTQI, robustness of the photonic HOTQI, and MAM in phononic quasicrystals.

[54] J. Lu, C. Qiu, L. Ye, X. Fan, M. Ke, F. Zhang, and Z. Liu, "Observation of topological valley transport of sound in sonic crystals," *Nat. Phys.* **13**(4): 369–374 (2017).

[55] B. Yan, Y. Peng, J. Xie, Y. Peng, A. Shi, H. Li, F. Gao, P. Peng, J. Jiang, F. Gao, J. Liu, and S. Wen, "Multifrequency and multimode topological waveguides in Stampfli-triangle photonic crystal with large valley Chern numbers," *arXiv:2104.14142*.

[56] Y. Hong, G. Tang, R. Peng, R. Fan, Z. Ma, Z. Wang, Y. Jiang, L. Chen, and M. Wang, "Direct observation of terahertz topological valley transport," *Opt. Express* **30**(9): 14839–14850 (2022).

[57] L. Yang, G. Li, X. Gao, and L. Lu, "Topological-cavity surface-emitting laser," *Nat. Photon.* **16**(4): 279–283 (2022).

[58] B. Hu, Z. Zhang, H. Zhang, L. Zheng, W. Xiong, Z. Yue, X. Wang, J. Xu, Y.

Cheng, X. Liu, and J. Christensen, “Non-Hermitian topological whispering gallery,” *Nature*, **597**(7878): 655–659 (2021).